ASME Journal of Verification, Validation and Uncertainty Quantification
Online journal at:
https://asmedigitalcollection.asme.org/verification

Juan D. Colmenares F[1]
Mechanical Engineering Department,
University of New Mexico,
Albuquerque, MN 87131
e-mail: colmenaresj@fusion.gat.com

Mohamed Abuhegazy
Mechanical Engineering Department,
University of New Mexico,
Albuquerque, MN 87131
e-mail: mabuhegazy@unm.edu

Yulia T. Peet
Mem. ASME
School for Engineering of Matter,
Transport and Energy,
Arizona State University,
Tempe, AZ 85281
e-mail: ypeet@asu.edu

Scott M. Murman
NASA Ames Research Center,
Moffett Field, CA 94035
e-mail: scott.murman@nasa.gov

Svetlana V. Poroseva[2]
Mem. ASME
Mechanical Engineering Department,
University of New Mexico,
Albuquerque, MN 87131
e-mail: poroseva@unm.edu

Sensitivity Analysis of Direct Numerical Simulation of a Spatially Developing Turbulent Mixing Layer to the Domain Dimensions

Understanding spatial development of a turbulent mixing layer is essential for many engineering applications. However, the flow development is difficult to replicate in physical or numerical experiments. For this reason, the most attractive method for the mixing layer analysis is the direct numerical simulation (DNS), with the most control over the simulation inputs and free from modeling assumptions. On the other hand, the DNS cost often prevents conducting the sensitivity analysis of the simulation results to variations in the numerical procedure and thus, separating numerical and physical effects. In this paper, effects of the computational domain dimensions on statistics collected from DNS of a spatially developing incompressible turbulent mixing layer are analyzed with the focus on determining the domain dimensions suitable for studying the flow asymptotic state. In the simulations, the mixing layer develops between two coflowing laminar boundary layers formed on two sides of a sharp-ended splitter plate of a finite thickness with characteristics close to those of the untripped boundary layers in the experiments by Bell and Mehta, AIAA J., 28(12), 2034 (1990). The simulations were conducted using the spectral-element code Nek5000.
[DOI: 10.1115/1.4062770]

Introduction

Turbulent mixing layers formed between two parallel streams of different velocities have long been studied due to their important role in various applications [1–6]. However, accurate prediction of such flows remains a challenge due to high sensitivity of their physics to variations in the flow parameters [7–11]. Even in the controlled environment of wind tunnel experiments, initial flow conditions preceding the mixing layer formation are affected by numerous factors that are difficult to replicate at other experimental facilities and in numerical experiments [4,12–16]. Thus, repeatability of the initial flow conditions is a problem to be addressed first for this flow geometry, before further progress in the flow prediction can be expected.

Direct numerical simulation (DNS) is a good fit for this problem, as the simulation inputs are controlled and there are no uncertainties in the simulation results associated with turbulence modeling. The main issue of using this method is its high cost driven by the requirement for resolving the smallest turbulent scales [17]. Since real mixing layers usually develop in space, this spikes the simulation cost even higher as a computational domain has to be sufficiently large to ensure that the flow fully transits to turbulence within the domain and its development is unaffected by the domain boundaries.

As a result, only few DNS studies of a mixing layer were previously conducted [15,16,18–32], with the majority of them being focused either on early stages of the mixing layer development (transition and pairing) or on exploring self-similarity of its asymptotic state far downstream from the mixing layer origin. An interest in the asymptotic state originates from theoretical results [33] showing that the properly normalized mean flow and turbulence statistics have universal profiles independent of the streamwise location in this flow regime. However, there is no consensus based on simulation and experimental data about the turbulent mixing layer asymptotic state characteristics, self-similarity, and sustainability [1–3,7,10,11,14,28,34–38].

Another consequence of the DNS high cost is that the sensitivity analysis of simulation results to the numerical procedure parameters is rarely performed. This makes it difficult to separate numerical and physical effects. In previous DNS of a spatially developing mixing layer, the sensitivity analysis was limited, for example, to effects of inflow perturbations [19] and those of the splitter plate thickness and the shape of its trailing edge [20]. Effects of the domain dimensions

[1]Present address: General Atomics, 3550 General Atomics Court, San Diego, CA 92121.
[2]Corresponding author.
Manuscript received January 4, 2023; final manuscript received June 14, 2023; published online July 17, 2023. Assoc. Editor: Yassin A. Hassan.

were previously found to be substantial in large eddy simulation of the flow [39–41]. This was later confirmed in DNS of this flow as well [18,42]. In Refs. [18] and [42], effects of the sharp-ended splitter plate thickness, characteristics of the laminar boundary layers used to form a mixing layer, temporal discretization scheme, and time-step were also investigated.

This study advances our previous works [18,42] with the goal of better understanding requirements for the computational domain dimensions in all three directions in DNS of a spatially developing mixing layer. To highlight the major differences in our current and previous studies, effects of the spanwise domain dimension were analyzed in Ref. [18] in a flow where boundary layers were separated by the infinitely thin plate. In this study, the effects are studied in the flow with the splitter plate of a finite thickness in a larger domain discretized using a finer grid. Two of the three cases considered in Ref. [42] were run again for this study with different initial conditions and longer to improve the quality of collected statistics for the analysis of the domain dimension in the transverse direction. The simulation time of the case with the largest domain in the streamwise direction from Ref. [42] was increased more than three times for this study to improve the data quality and strengthen the conclusions. A better insight into the grid resolution effects was also sought in this study as the secondary objective. In addition, the data analysis was extended to include the fully turbulent mixing layer region far from the splitter plate not covered in Ref. [42] to facilitate future studies of the flow asymptotic state.

In the simulations, the mixing layer spatially develops from two coflowing laminar planar boundary layers formed on two sides of the splitter plate, with the boundary layer conditions closely matching those in experiments with untripped boundary layers [11,37]. No artificial flow perturbation is applied at any stage of the flow development. Instead, the splitter plate of a finite thickness is utilized. This is sufficient to trigger the mixing layer transition to turbulence [16,18]. Moreover, this feature is present in any experiments and is easy to replicate in simulations.

The spectral-element method [43] implemented in the Nek5000 code [44] was used in the study to conduct simulation.

Numerical Procedure

In the simulations, the Nek5000 BDF3-OIFS temporal-discretization scheme is utilized that uses a characteristics-based time-stepping scheme for nonlinear terms in combination with the operator-integration factor scheme (OIFS) of the third-order accuracy and the implicit third-order backward difference scheme (BDF3) for viscous terms. The scheme allows for time steps larger than those required by conventional explicit approaches [44]. In this study, $\Delta t = 0.02$ in all simulations are based on our previous analysis [42]. (In the simulations, t is nondimensional time, normalized with respect to U_1 and δ_1, and so are all time intervals.) This yields CFL = 0.75 in cases I–III and CFL = 1.8 in cases IV–VI described below, where CFL is the Courant–Friedrichs–Levy parameter, $|\mathbf{u}|\Delta t/\Delta x$, and Δx is the grid spacing in the global coordinates between the Gauss–Legendre–Lobatto quadrature points inside the elements. Locations of the internal points correspond to the roots of a locally defined polynomial $L'_N(x)$, where $L_N(x)$ is a Legendre polynomial of order N. Polynomial interpolants of order $N = 11$ are used in all simulations. Time, lengths, and velocities in this paper are normalized with respect to the value of U_1 and δ_1 from Ref. [11], which are the high-speed freestream velocity and the boundary layer thickness at the splitter plate trailing edge, respectively. Additional details of the numerical procedure are provided in Refs. [42] and [44].

Six computational domains (cases I–VI) were used in the simulations as described in Table 1. All domains have a similar cross section in the (x,y)-plane shown in Fig. 1. In the figure, the thick black line represents the splitter plate and thin lines indicate other boundaries of the domain. The sharp-ended splitter plate is uniform, with its thickness being $0.0625\delta_1$. High- and low-speed boundary layers develop on the top and bottom sides of the plate, respectively. The plate has different lengths on its different sides: $L_1/\delta_1 = 175$ and $L_2/\delta_1 = 140$, [18,42] to closely match the experimental boundary layers conditions at the splitter plate trailing edge [11]. A region of the length $L_3/\delta_1 = 10$ is added upstream of the splitter plate to avoid the singularities in the boundary conditions.

The trailing edge of the plate is located at $x = 0$. Positive x-values are in the region, where two boundary layers mix (thereafter, mixing region). The mixing region length, L_x/δ_1, varies in the simulations between 170 and 350 (Table 1). To compare, the mixing region length of the test section in the experiments [11] was $915\delta_1$, with self-similarity being observed in some flow characteristics by $L_x/\delta_1 \sim 312.5$.

The y-values are negative in the lower part of the domain and positive in its upper part, with $y = 0$ being located at the splitter plate bottom in cases I–III and at the middle of the splitter plate in cases IV–VI due to different grids used in these cases (see discussion in the Grids section). Minimum and maximum y-values correspond to $\pm L_y/2$, where L_y is the domain dimension in the transverse direction. The largest value of L_y, $90\delta_1$, corresponds to the length of the experimental test section, 36 cm, in this direction [11].

The z-values run from 0 to L_z between the domain boundaries, where L_z is the domain dimension in the spanwise direction. The largest dimension of the computational domain in the spanwise dimension is $40\delta_1$. The wind tunnel test section size in this direction was $227.5\delta_1$. A small difference in L_z in cases III and VI is due to different grids used in these cases.

The standard Nek5000 boundary conditions are used in all simulations. They are shown in Fig. 1. The no-slip boundary condition is applied everywhere on the splitter plate. The symmetry condition is applied at the lower boundary of the region upstream of the splitter plate. The convective outflow condition is applied at the outlet and at the lower boundary of the domain. The outflow-normal condition is applied at its upper boundary. This condition implies that the velocity component normal to the boundary is free ($\partial V/\partial n = 0$), but the tangential velocity components are fixed: $U = U_1/U_\infty$ and $W = 0$. The outflow conditions ensured that the mean pressure gradient is negligible in the streamwise direction: the pressure change across the mixing layer region, $\langle p\rangle(x = L_x) - \langle p\rangle(x = 0)$, is $\sim 0.016\,\rho U_1^2$ at the flow centerline and $\sim 0.0016\,\rho U_1^2$ in the freestream. In the spanwise direction, the periodic boundary conditions are used.

At the inlet, the following velocity profiles are assigned:

$$U(x = x_{\text{inl}},\, y,\, z,\, t) = \begin{cases} U_1/U_\infty = 1, \text{ if } y > 0 \\ U_2/U_\infty = 0.6, \text{ if } y < 0 \end{cases} \qquad (1)$$
$$V(x = x_{\text{inl}}, y, z, t) = W(x = x_{inl}, y, z, t) = 0$$

where x_{inl} is the location of the inlet boundary. Velocity profiles (1) are used throughout the domain as initial conditions in all cases but case III, where the velocity field was interpolated from case I at $|y/\delta_1| < 35$ and velocity profiles (1) were used at $|y/\delta_1| > 35$. This was done to accelerate simulations.

Grids

Two base grids are used in the simulations: one for cases I–III and the other for cases IV–VI. The grids are shown in Figs. 2(*a*) and 2(*b*),

Table 1 Computational domain dimensions

Case	Description	L_x/δ_1	L_y/δ_1	L_z/δ_1
I	Small domain	170	2×35	23.4
II	Small domain reduced in y	170	2×25	23.4
III	Small domain extended in y	170	2×45	23.4
IV	Large domain	350	2×45	40.0
V	Large domain reduced in x	170	2×45	40.0
VI	Large domain reduced in x and z	170	2×45	23.56

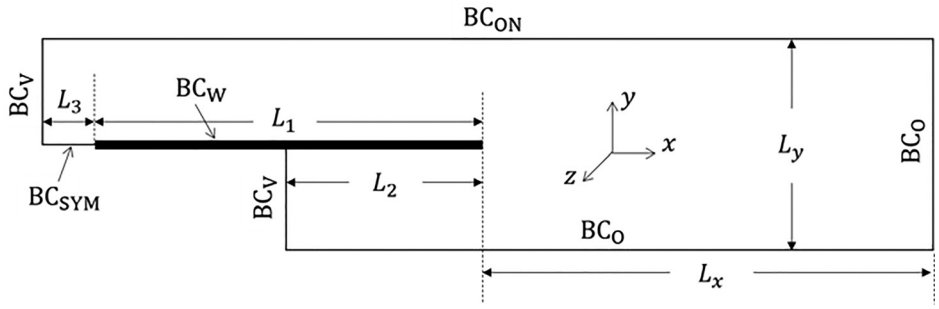

Fig. 1 Computational domain geometry and the boundary conditions: BC_O—outflow, BC_{ON}—outflow/normal, BC_V—uniform velocity, BC_W—wall (no-slip), and BC_{SYM}—symmetry (free-slip)

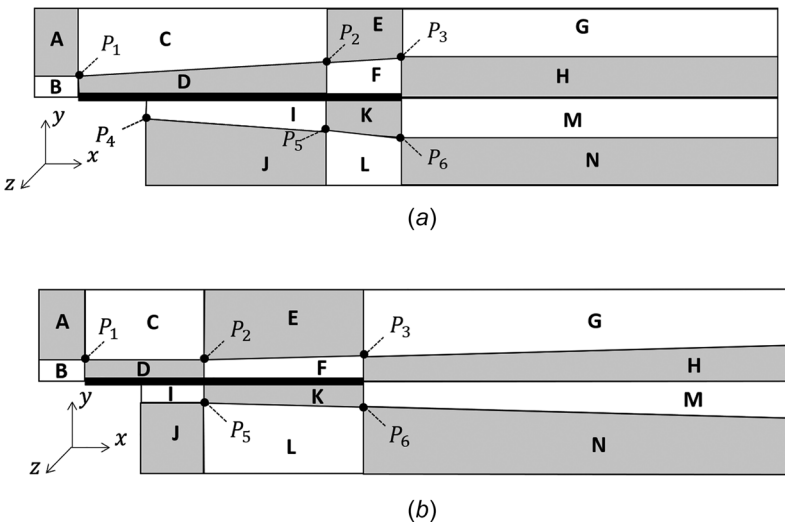

Fig. 2 Meshing zones for the base grids: (*a*) cases I–III and (*b*) cases IV–VI (not to scale)

respectively, in terms of conforming meshing zones in the (x,y)-plane. Details on the grid generation are provided in the Supplement Material on the ASME Digital Collection (see also Ref. [42]). Overall, the area downstream of the splitter plate is more refined in the base grid for cases IV–VI (Fig. 2(*b*)) than in the base grid used in the cases I–III simulations (Fig. 2(*a*)). The grid resolution near the splitter plate trailing edge is shown for both grids in Fig. 3 for comparison. Typical grid resolution in DNS follows $(\delta x \cdot \delta y \cdot \delta z)^{1/3} \sim 4\eta_K \div 8\eta_K$ [45–48], where $\delta x, \delta y, \delta z$ is the average spacing between quadrature points within the grid elements in the streamwise, transverse, and spanwise directions, η_K is the Kolmogorov length scale: $\eta_K = \left(\nu^3/\varepsilon\right)^{1/4}$. In this study, the grid resolution in cases I–III is $(\delta x \cdot \delta y \cdot \delta z)^{1/3} < 5.33\,\eta_K$, while in cases

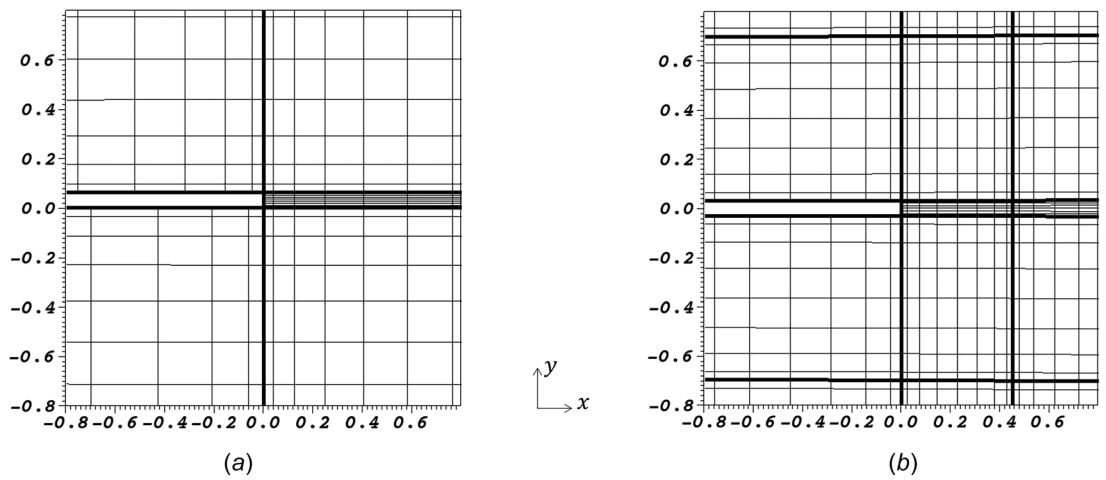

Fig. 3 Spectral element grid (thick lines) and quadrature points (intersection of thin lines) near the trailing edge of the plate in the base grids for (*a*) cases I–III and (*b*) cases IV–VI

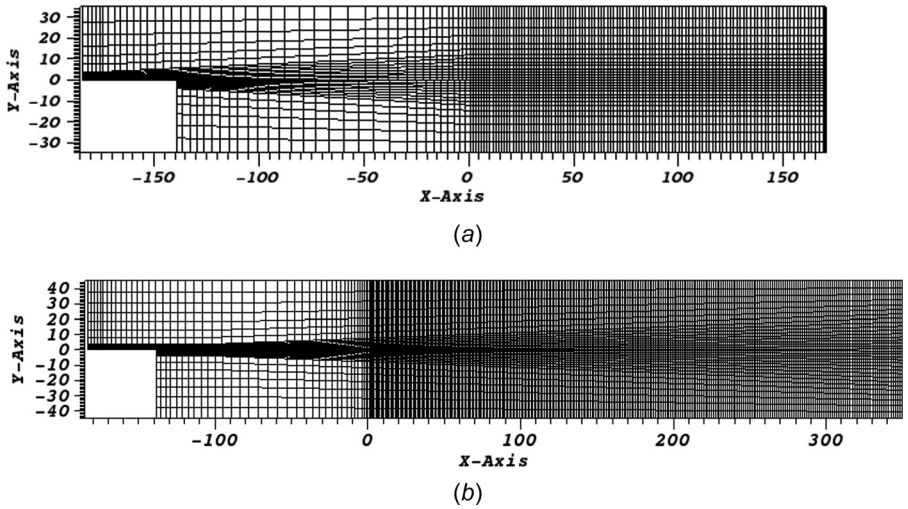

Fig. 4 Base grids of spectral elements (without internal collocation points): (*a*) cases I–III and (*b*) cases IV–VI

IV–VI, it is $(\delta x \cdot \delta y \cdot \delta z)^{1/3} < 4.9\,\eta_K$, everywhere in the flow. The grid resolution in the individual directions is: $\delta x < 5.65\eta_K$, $\delta y < 5.31\eta_K$, and $\delta z < 5.05\eta_K$ in cases I–III, and $\delta x < 5.18\eta_K$, $\delta y < 4.53\eta_K$, and $\delta z < 5.08\eta_K$ in cases IV–VI.

In the spanwise direction, the grids used in cases I–III have twenty uniformly distributed elements of the size $\Delta z/\delta_1 = 1.17$. The total numbers of grid elements in cases I–III are: 84,800, 73,000, and 96,600, respectively.

The base grid shown in Fig. 2(*b*) is used in the case IV simulations. This grid is modified by cutting it off at $x/\delta_1 = 170$ to obtain the grid used in the case V simulations. The grids for cases IV and V have 34 uniformly distributed elements in the spanwise direction, with their size being $\Delta z/\delta_1 = 1.178$ in this direction. The total numbers of the grid elements in cases IV and V are 381,174 and 233,070, respectively.

The grid for case VI was obtained from the case V grid by cutting it off at $z/\delta_1 = 23.56$, which is the closest point near the location of the grid boundary in case I ($L_z/\delta_1 = 23.4$). Then, the grid was remeshed in this direction to include 20 uniformly distributed elements with $\Delta z/\delta_1 = 1.178$. The total number of grid elements in case VI is 137,100.

The base grids from Fig. 2 that include only spectral elements without collocation points are shown in Fig. 4. The number of quadrature points located inside each element is $(N+1)^3$, with the $N+1$ quadrature points being located in each direction based on the distribution of Gauss–Legendre–Lobatto quadrature points in local (elemental) coordinates and $N = 11$ as specified above.

Flow Conditions

The flow conditions were specified to closely match those for the untripped boundary layers before their mixing downstream of the splitter plate in the wind tunnel experiments of Bell and Mehta [11,37] (Table 2). However, without further advances in experimental and computational methods, differences between the experimental and simulation inputs and as a result, in their outputs are expected as discussed in Ref. [42]. Here, we just mention that in the experiments [11,37], the untripped boundary layers were neither exactly laminar nor planar prior mixing, which is in contrast to the boundary layers obtained at the trailing edge of the splitter plate in our simulations. Tables 2 and 3 provide some of the boundary layers characteristics observed in the experiments and the simulations. In particular, the boundary layer thickness and the momentum thickness at the splitter plate trailing edge achieved in our simulations are within 1.5% and 2.5% of the corresponding experimental values on both sides of the splitter plate. The corresponding Reynolds numbers in the simulations are close to those in the experiments. Variations in the boundary layer characteristics presented in Table 3 do not exceed 1% for all cases considered in the paper.

The accuracy of the experimental data is given in Ref. [37] in terms of the freestream velocities being within 1% of nominal values and the repeatability of the Reynolds stress measurements being 5%.

Even though differences in the results from the experiments and the simulations are expected, their comparison is still beneficial for identifying those flow parameters that are less sensitive to the input differences and thus, more reliable from the perspective of the flow physics analysis. Future studies on the sensitivity analyses of DNS results to other numerical parameters will benefit from such a comparison as well. For these reasons, experimental data (where available) are provided in the figures in the Results section and in the Supplemental Materials on the ASME Digital Collection.

Collection of Statistics

The same procedure as in Ref. [42] is used in this study to collect statistics. That is, ensemble-averaged statistics, $\langle Q\rangle_{\text{en}} = \langle Q\rangle_{\text{en}}(x,y,z)$, were first extracted using N_s number of flow realizations or "snapshots." In cases I–III, V, and VI, $N_s = 376$ was used. The number of snapshots used in case IV was $N_s = 529$. The ensemble-averaged data were further averaged in the spanwise direction

$$\langle Q\rangle = \langle Q\rangle(x,y) = \frac{1}{L_z}\int_0^{L_z} \langle Q\rangle_{\text{en}}(x,y,z)dz \tag{2}$$

to improve the statistics quality and to obtain statistics for the planar flow.

Table 2 Experimental boundary layer characteristics near the splitter plate trailing edge

Splitter plate side	U_∞, m/s	δ_{99}/δ_1	θ/δ_1	Re_δ	Re_θ
High-speed side	15	1	0.1325	3962	525
Low-speed side	9	1.1	0.1525	2611	362

Table 3 Simulated boundary layer parameters at the splitter plate trailing edge

Case	Splitter plate side	U_∞/U_1	δ_{99}/δ_1	θ/δ_1	Re_δ	Re_θ
I–VI	High-speed side	1	0.99	0.143	3930	565
I–VI	Low-speed side	0.6	1.01	0.153	2412	364

Statistical data were collected after an initial transient period, t_{trans}, determined by the volume-averaged flow kinetic energy, as shown in Fig. S1 available in the Supplemental Materials on the ASME Digital Collection. The nondimensional transient period was $t_{trans} = 500$ for all cases. This corresponds to 2.4 flow-through times $\tau_f = L_x/U_c$ in cases I–III, V, and VI, and to $1.15\tau_f$ in case IV.

Statistics for all cases, but case IV, were collected during the same number of flow-through times, $7.05\tau_f$. This corresponds to the time interval $t = [500, 2000]$ in cases I–III, V, and VI. In Case IV with the largest dimension L_x, data were collected during $12.1\tau_f$, which corresponds to the time interval $t = [500, 5780]$. This is about 3.5 times longer than reported in Ref. [42] and about twice of the time used in the other cases.

Convergence of the statistics has been achieved in all cases as shown in Figs. S2–S4 available in the Supplemental Materials. Considered statistics are mixing layer thickness, momentum thickness, and normal Reynolds stresses integrated across the mixing layer, all evolving in the streamwise direction. Profiles of the Reynolds stresses were also collected at selected locations.

In the study, the mixing layer thickness, δ_{ML}, is defined as in Ref. [11], and obtained by computing the least-squares fit of the mean velocity profile to the error function profile shape $(\langle U\rangle - U_2)/\Delta U \approx [1 + \mathrm{erf}(\eta)]/2$, where η is the normalized transverse coordinate

$$\eta = (y - y_0)/\delta_{ML} \tag{3}$$

Reynolds stresses integrated across a mixing layer are determined as

$$K_{x_i}(x) = \frac{1}{\Delta U^2}\int_{-L_y/2}^{L_y/2} \langle u_i^2\rangle \, dy \tag{4}$$

Notice that in Eq. (4), values inside the angle brackets are those already averaged in the spanwise direction.

A useful observation from the data analysis that we recommend for using as a criterion for the statistics convergence in this flow geometry is the convergence of $K_y(x)$ (see supplemental Fig. S3 available in the Supplemental Materials): its convergence guarantees convergence of other statistics.

Results

Transverse Dimension Effects. To investigate influence of the domain transverse dimension, L_y, on the flow solution, its value varied from $50\delta_1$ in case II to $70\delta_1$ and $90\delta_1$ in cases I and III, respectively. The largest L_y used in case III corresponds to the size of the experimental test section in this direction. Dimensions L_x and L_z are the same in the three cases: $L_x/\delta_1 = 170$ and $L_z/\delta_1 = 23.4$.

As shown in Fig. 5(*a*) and supplemental Fig. S5(*a*) available in the Supplemental Materials, the growth of the mixing layer thickness (and of the momentum thickness) is unaffected by variations in L_y, when $L_y \geq 50\delta_1$. The streamwise mean velocity profiles at different streamwise locations also do not vary with L_y in the three cases (supplemental Fig. S6a available in the Supplemental Materials). The location of the flow transition to turbulent (associated in this study with the value of the turbulent kinetic energy integrated across the mixing layer, K, becoming nonzero): $x/\delta_1 \cong 15$ (Fig. 6(*a*)), is also insensitive to variations in L_y at $L_y \geq 50\delta_1$.

Larger domain ($L_y \geq 70\delta_1$) is required to achieve independence of solutions for K and for the integrated Reynolds stress, K_x, of this domain dimension (Figs. 6(*a*) and 6(*b*)).

Statistics associated with the transverse direction such as, for example, K_y, continue to vary with L_y being increased (Fig. 6(*c*)). The profile of K_z adjusts (Fig. 6(*d*)) so that the behavior of K remains unchanged at $L_y \geq 70\delta_1$.

The analysis of one-point Reynolds stresses and turbulent kinetic energy profiles at various locations in the streamwise direction (supplemental Fig. S7 available in the Supplemental Materials) confirms the above observations. That is, the profiles of k and of $\langle u^2\rangle$ lose sensitivity to L_y at $L_y \geq 70\delta_1$ at all considered locations, but profiles of $\langle v^2\rangle$, $\langle w^2\rangle$, and $\langle uv\rangle$ continue to vary when the domain dimension L_y/δ_1 changes from 70 to 90. The Reynolds stresses $\langle w^2\rangle$

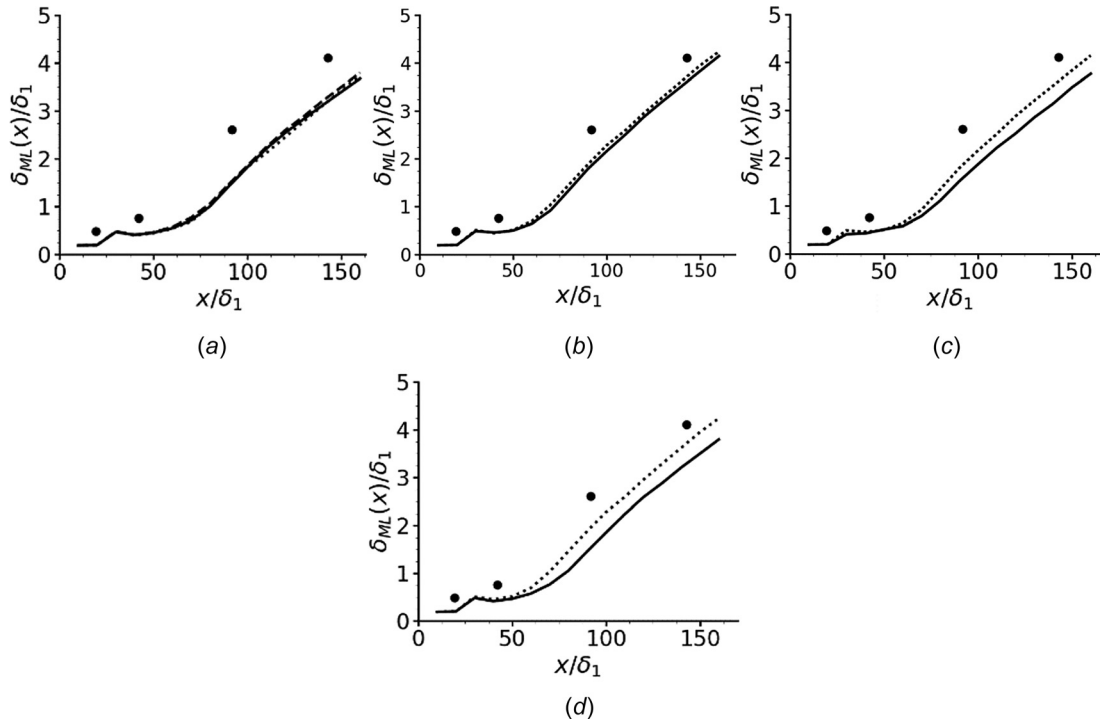

Fig. 5 Streamwise evolution of the mixing layer thickness: (*a*) — case I, · · · · case II, - - - case III, (*b*) — case V, · · · · case VI, (*c*) — case IV, · · · · case V, (*d*) — case III, · · · · case VI; circles are data from experiment [11] on all plots

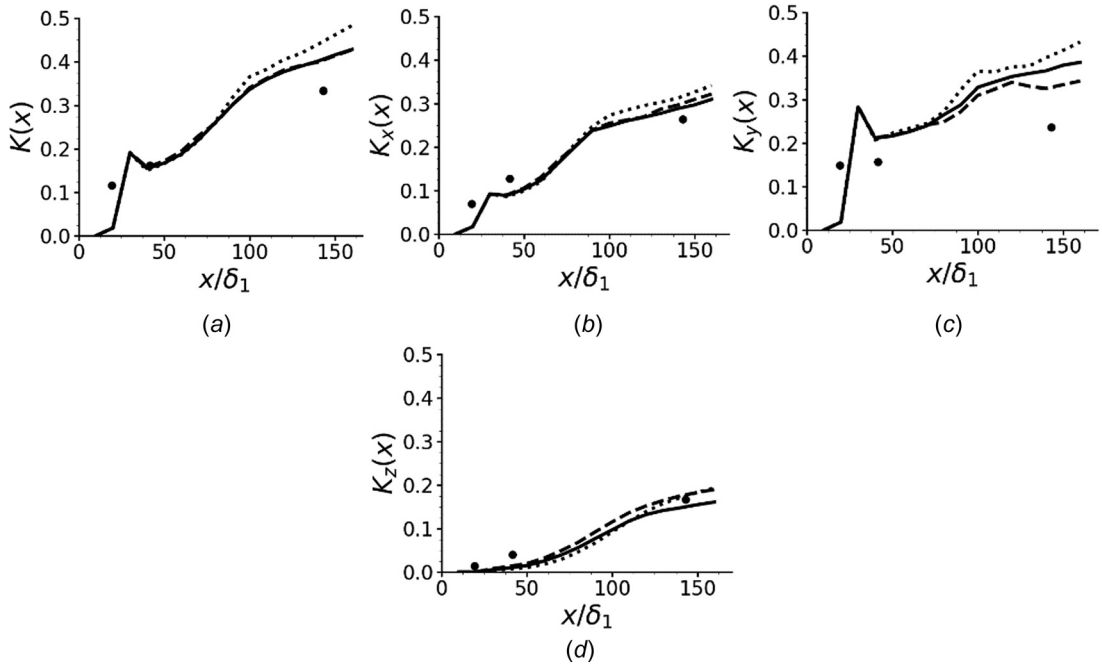

Fig. 6 Streamwise evolution of the flow characteristics integrated across the mixing layer in cases I–III. Notations are the same as in Fig. 5(*a*).

and $\langle uv \rangle$ show dependence on this domain dimension at all considered locations. For $\langle v^2 \rangle$, the effect is more pronounced when the mixing layer is fully turbulent.

To summarize, the domain dimension in the transverse direction of $70\delta_1$ is sufficient to ensure independence of scalar statistics and those associated with the streamwise direction of this domain dimension. Larger domain is required for statistics associated with the transverse and spanwise directions. The analysis of one-point statistics is not conclusive that $L_y/\delta_1 = 90$ is sufficient for this purpose.

Two-point spatial correlations $R_{ij}(r_y) = \langle u_i(y)u_j(y+r_y)\rangle$ in the transverse direction were also collected in the study to clarify this matter further. However, due to limited resources, they were only collected in case IV with the largest domain in all directions including in the transverse direction: $L_y/\delta_1 = 90$. In Fig. 7, $R_{ij}(r_y)$, with $r_y = 0$ corresponding to the point $(x, y, z) = (320\delta_1, 0, 0)$ are shown normalized by their values at $r_y = 0$. The figure confirms that the correlations involving velocity fluctuations in the transverse direction: R_{yy}, R_{yx}, and R_{xy} have the largest length scales in this direction close to a half of the domain dimension $L_y/\delta_1 = 90$. In the case of R_{xy} and R_{yy}, the length scales may slightly exceed that or these are effects of the domain boundary conditions. For future studies, our recommendation is to first investigate a role of the boundary conditions imposed on the domain boundary in the transverse direction prior increasing the domain dimension further in this direction. (The correlation profiles were statistically converged as demonstrated in supplemental Fig. S8 available in the Supplemental Materials on the ASME Digital Collection.)

Notice also that in cases I–III, the computational domain dimension L_y satisfies and exceeds the criterion

$$6.96 < L_y/\delta_{\omega,\max} < 8.3 \tag{5}$$

used in Refs. [21] and [22] to ensure the solution independence of this domain dimension. In our simulations, $L_y/\delta_{\omega,\max} = 11.25, 8.03$, and 14.75 in cases I, II, and III, respectively (see also supplemental Table S5 available in the Supplemental Materials, which provides

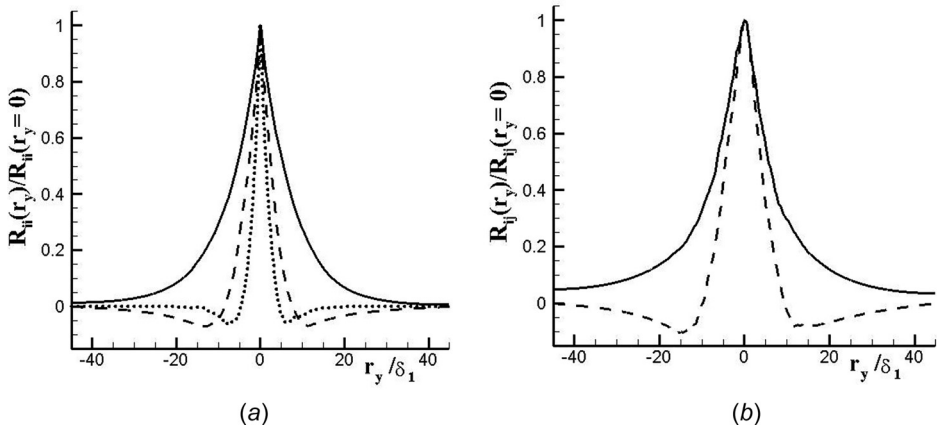

Fig. 7 Two-point correlations in the transverse direction with r_y=0 at point (x, y, z)=(320δ_1, 0,0) in the case IV simulations: (*a*) *i*=*j*, (*b*) $i \neq j$. Notations: (*a*) - - - R_{xx}, — R_{yy}, · · · · R_{zz}, (*b*) — R_{xy}, - - - R_{yx}.

this ratio value in all cases). Our study shows that this criterion does guarantee independence of the mean flow characteristics from the transverse domain dimension, but not of the turbulence statistics.

Spanwise Dimension Effects. Previously, effects of the spanwise domain dimension on results of DNS of a mixing layer were studied in Ref. [18], and it was shown that two Reynolds stresses—$\langle uv \rangle$ and $\langle w^2 \rangle$—were mainly affected by variations in L_z and particularly, toward the domain exit. In Ref. [18], two domains were used in those simulations: one domain had the same dimensions as the Case I domain of this study with $L_z/\delta_1 = 23.4$, and the other domain with the same values of L_x and L_y as in the case I domain (Table 1), but with L_z twice increased: $L_z/\delta_1 = 46.8$. (In the experiments [11], the test section dimension in the spanwise direction was $L_z/\delta_1 = 227.5$.)

Two plates were used in Ref. [18] to generate the boundary layers: infinitely thin and of a finite thickness. The plate thickness was found to have a strong impact on the mixing layer development [18]. For this reason, in this study, we consider sensitivity of the simulation results to L_z in the mixing layer simulations with the splitter plate of a finite thickness. Simulations with two values of L_z were conducted for this purpose: $L_z/\delta_1 = 40$ (case V) and $L_z/\delta_1 = 23.56$ (case VI) (Table 1). The domain dimension in the transverse direction was increased to $L_y/\delta_1 = 90$ in both cases following the results presented in the section. In Ref. [18], $L_y/\delta_1 = 70$.

The simulation results confirm those in Ref. [18] that at $L_z/\delta_1 > 23.4$, the integrated flow characteristics and the streamwise mean velocity are affected little if at all by this domain dimension (Figs. 5(*b*) and 8, also supplemental Figs. S5(*b*) and S6(*b*) available in the Supplemental Materials on the ASME Digital Collection), with the exception of $K_z(x)$, which grows faster in case V (Fig. 8(*d*)) in the area far from the splitter plate ($x/\delta_1 > 125$). Similar tendency is observed in the profile of the Reynolds stress $\langle w^2 \rangle$ associated with the spanwise direction: its maximum value increases toward the domain exit in Case V to compare with Case VI (Fig. 9).

Other Reynolds stresses are unaffected by variations in L_z when the mixing layer is turbulent, but are sensitive to this parameter in the domain area close to the splitter plate, with $\langle uv \rangle$ being the most affected. There is negligible effect on $\langle w^2 \rangle$ by L_z in this flow area (Fig. 9). These observations are also consistent with those reported in Ref. [18].

Thus, one can infer that regardless of the splitter plate thickness and the increase of the domain dimension in the transverse direction, the Reynolds stress $\langle w^2 \rangle$ remains sensitive to L_z toward the domain exit. The flow transition area in the (x, y)—plane is also sensitive to variations in L_z within the considered range of this parameter.

Notice that in this study, the value of L_z satisfies the criterion

$$A = L_z/\theta_{\max} > 10 \tag{6}$$

in all cases (supplemental Table S6 available in the Supplemental Materials). Criterion (6) was proposed in Ref. [39] for the simulation results to be independent of L_z. Results of our simulations show that this criterion does not guarantee independence of turbulence statistics associated with the spanwise direction when the flow is turbulent. The flow transition area is also affected. In Refs. [37] and [49–52], observations were made about existence of nondiminishing two-point correlations in the spanwise direction indicating a presence of the mixing layer spanwise structure. Similar results were obtained in this study for such correlations (supplemental Fig. S9 available in the Supplemental Materials). This could be one of possible explanations for observed effects. It also shows that two-point correlations are not suitable for evaluating the domain dimension adequacy in the spanwise direction in this flow geometry.

Streamwise Dimension Effects. Results from the cases IV and V simulations are used in this subsection to analyze the impact of variation of the domain streamwise dimension on the mixing layer development. In case IV, the domain exit is located at $x/\delta_1 = 350$ and in case V, at $x/\delta_1 = 170$. Data for the two cases are compared at $x/\delta_1 < 170$. The size of the experimental test section in this direction was $915\delta_1$ [11].

The simulation results show that the mixing layer grows faster in the shorter domain of case V (Fig. 5(*c*) and supplemental Fig. S5(*c*) available in the Supplemental Materials) at $x/\delta_1 > 50$ during the flow transition to turbulence. The flow transition also starts closer to the splitter plate in the shorter domain: at $x/\delta_1 \approx 15$ compared with $x/\delta_1 \approx 25$ in case IV (Fig. 10(*a*)).

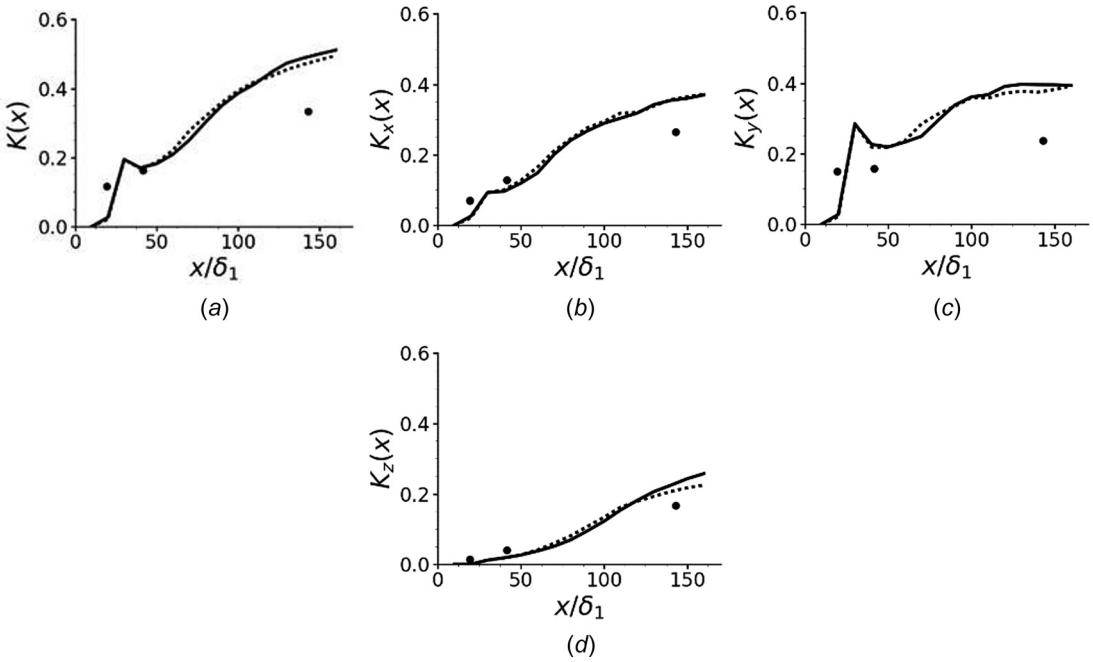

Fig. 8 Streamwise evolution of the flow characteristics integrated across the mixing layer in cases V and VI. Notations: — case V, · · · · case VI.

The streamwise mean velocity profiles in supplemental Fig. S6(*c*) available in the Supplemental Materials on the ASME Digital Collection provide an explanation for a faster growth of the mixing layer in the shorter domain of case V. Specifically, the wake effect of the splitter plate vanishes more rapidly in the shorter domain, which implies the flow mixing starting sooner in this case. Far from the splitter plate, the streamwise mean velocity profile is the same as in all other cases.

Solutions for the integrated parameters K, K_x, and K_y are close in both cases at $x/\delta_1 \leq 125$, except for the flow area of early transition to turbulence, with the difference between the solutions being observed around $x/\delta_1 \sim 40$. At $x/\delta_1 > 125$, the growth of these parameters slows down in the shorter domain of Case V, which implies the effect of the domain exit. The behavior of K_z is affected by L_x everywhere in the domain: its growth rate is noticeably higher in the shorter domain of case V (Fig. 10(*d*)).

Comparing results in Fig. 10 with those in Figs. 6 and 8, one can notice that the growth rates of all four parameters: K, K_x, K_y, and K_z tend to slow down at $x/\delta_1 > 125$ when the domain dimension in the streamwise direction is limited to $L_x/\delta_1 = 170$. Thus, this effect is likely due to the domain exit proximity in addition to other effects caused by variations in the domain dimensions. The domain exit effect seems to be sensitive to L_x as well, as it disappears when the domain dimension in the streamwise direction is increased to $L_x/\delta_1 = 350$ (case IV) (see more discussion of this case in the Domain Dimensions for the Flow Self-Similarity Study section).

With the domain exit effect in mind, one can infer from Fig. 10 that the parameter K_z is the only one strongly affected by L_x: its growth rate is higher in the turbulent mixing layer in the simulations with the shorter domain (case V).

The Reynolds stress profiles (Fig. 11) confirm that transition to turbulence occurs sooner in case V (the shorter domain), which is indicated by higher maximum values of $\langle u^2 \rangle$ and $\langle v^2 \rangle$ in the area close to the splitter plate.

Far away from the splitter plate, profiles of $\langle u^2 \rangle$, $\langle v^2 \rangle$, and $\langle w^2 \rangle$ agree with the observations for corresponding integrated parameters. In particular, reduction in the maximum values of $\langle u^2 \rangle$ and $\langle v^2 \rangle$ should be considered as the domain exit effect rather than that of L_x. The $\langle uv \rangle$-profiles are the same in cases IV and V in the turbulent part of the mixing layer, but toward the splitter plate trailing edge, this Reynolds stress is affected by L_x as other Reynolds stresses do.

Strong influence of the domain streamwise dimension on the mixing layer development was observed in Ref. [36], where it was suggested that large vortex structures near the experimental outlet boundary may be coupled to small structures upstream, producing a feedback mechanism between upstream and downstream flows. This makes the mixing layer structure and its development dependent on the streamwise size of the experimental test section and complicates formulating the boundary conditions at the domain exit in simulations. Results from our simulations show that not all considered parameters are affected by variations in L_x and that effects of this domain dimension differ depending on the flow area.

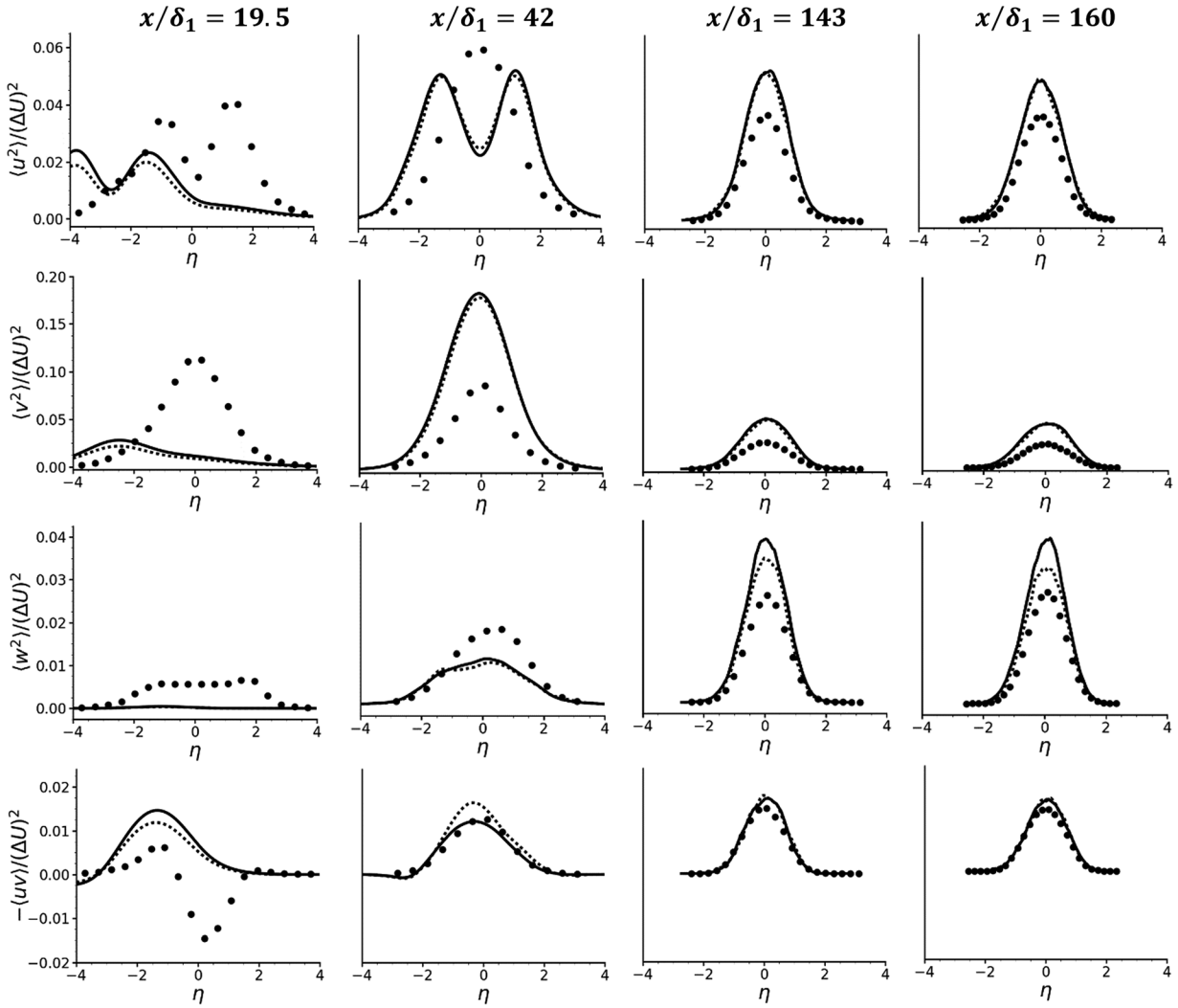

Fig. 9 Profiles of the Reynolds stresses at different locations in the streamwise direction for cases V and VI. Notations: — case V, · · · · case VI.

Specifically, when the mixing layer is turbulent, parameters associated with the spanwise direction, K_z and $\langle w^2 \rangle$, and those characterizing the mixing layer growth, δ_{ML} and θ_{ML}, are affected by L_x. In the areas of the splitter plate wake and the flow transition to turbulence, all parameters are sensitive to this domain dimension.

Grid Effects. The grid effects on the simulation results were not a focus of this study. However, since two base grids were used in the simulations, some of these effects were analyzed using data from cases III and VI. In the two cases, the domain dimensions in the (x, y)—plane are equivalent. In the spanwise direction, the domain dimensions are very close: $L_z/\delta_1 = 23.4$ in case III versus 23.56 in case VI, with the number of grid elements being the same in this direction in both cases. The Case VI grid is finer in the (x, y)—plane in the splitter plate wake (Grids section).

Results for the two cases are compared in Figs. 5(*d*) and 12, also in supplemental Figs. S5(*d*) and S10 available in the Supplemental Materials on the ASME Digital Collection. They show that streamwise evolution of all considered integrated parameters is strongly sensitive to the grid, with the growth rate of all of them being higher in Case VI, when the grid is finer (dotted lines in the figures). Differences appear at $x/\delta_1 > 30$ during the flow transition to turbulence.

The streamwise mean velocity profiles show no sensitivity to the grid resolution (supplemental Fig. S6(*d*) available in the Supplemental Materials).

The grid resolution effect on the Reynolds stresses is weaker than on the integrated parameters, but the tendency is the same, that is, the maximum values of the Reynolds stresses are slightly higher in case VI with a finer grid (supplemental Fig. S10 available in the Supplemental Materials).

The difference in the strength of the grid effect on the Reynolds stresses and on the corresponding integrated parameters is an indication of a larger contribution of the flow area outside the $\pm 3\eta$ range into the integrated parameters when the finer grid is used. Preliminary results showed that the grid stretching in the transverse direction is a factor affecting the simulation results in both cases. Due to resource constraints, a comprehensive analysis of this and other grid effects is left for future studies.

Domain Dimensions for the Flow Self-Similarity Study. One of the research objectives of this study was to determine the domain dimensions where a mixing layer can potentially reach the asymptotic state. The in-depth analysis of such a state is not the objective of this study and will be presented elsewhere.

As the first step, the one-dimensional energy spectrum [49]

$$E_{xx}(\omega) = \frac{1}{\pi}\int_{-\infty}^{\infty} e^{-i\omega\tau} R_{xx}(\tau)\, d\tau = \frac{1}{\pi}\int_{-\infty}^{\infty} e^{-i\omega\tau}\langle u(t)u(t+\tau)\rangle\, d\tau, \tag{7}$$

was computed at various x-locations at $y = 0$ in the domains with $L_x/\delta_1 = 170$ and 350. The constant slope of –5/3 was used to determine if the flow is fully turbulent at a given location. As an example, spectra obtained in the case I simulations with $L_x/\delta_1 = 170$ are shown in supplemental Fig. S11 available in the Supplemental Materials at two locations: $x/\delta_1 = 100$ and 150. As the figure demonstrates, the flow is transitional at $x/\delta_1 = 100$ and fully turbulent at $x/\delta_1 = 150$ in this case.

In the largest domain of case IV, the inertial range is still under development at $x/\delta_1 = 150$ (Fig. 13(*a*)), which supports the observation made earlier that the turbulence development is delayed by increasing the domain dimension in the streamwise direction. Further downstream, the flow becomes fully turbulent. An example of the spectrum in this part of the flow is shown in Fig. 13(*b*) at $x/\delta_1 = 325$. Thus, the mixing layer becomes fully turbulent in both domains with $L_x/\delta_1 = 170$ and 350.

Several criteria were suggested in the past to identify if a turbulent mixing layer has reached its asymptotic state. The least restrictive criterion is based on the behavior of streamwise mean velocity. The asymptotic profile of this mean flow characteristic has been achieved by $x/\delta_1 = 160$ in all simulations (supplemental Fig. S6 available in the Supplemental Materials).

Another criterion is the linear growth of the mixing layer thickness [11]. In case IV, this is observed at $x/\delta_1 > 180$ (Fig. 14(*a*)). In the figure, the dashed line corresponds to the constant slope and the solid line is the simulation result. This criterion is also applicable to other cases at $x/\delta_1 > 125$ (Fig. 5), but the domain exit effects discussed earlier have to be kept in mind.

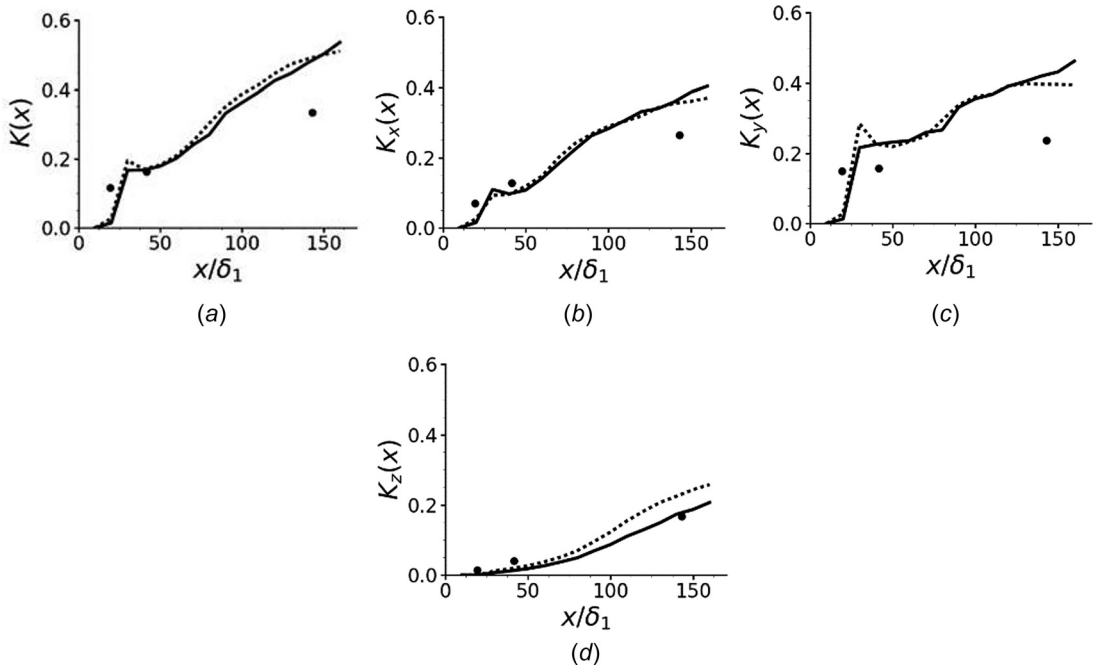

Fig. 10 Streamwise evolution of the flow characteristics integrated across the mixing layer in cases IV and V. Notations: — case IV, · · · · case V.

Turbulence statistics are expected to become independent of the streamwise location in the turbulence asymptotic state when normalized with respect to the mixing layer thickness and the velocity difference, ΔU [8,11,49]. For K, this requirement is equivalent to the linear growth with the distance downstream of the splitter plate [22]. Figure 14(*b*) demonstrates that this is indeed the case at $x/\delta_1 > 180$ in the case IV simulations. In simulations with shorter domains, the linear growth of K is observed at $x/\delta_1 > 130$ (Figs. 6(*a*), 8(*a*), and 10(*a*)), but as with the mixing layer thickness, turbulent statistics are affected by the domain exit in this flow area. For this reason, domains with $L_x/\delta_1 = 170$ are deemed unsuitable for the turbulence asymptotic state study.

Streamwise evolution of the Reynolds stress profiles obtained in case IV is shown in supplemental Fig. S12 available in the Supplemental Materials on the ASME Digital Collection. Profiles of $\langle u^2 \rangle$ and $\langle v^2 \rangle$ vary little between $x/\delta_1 = 280$ and 320. However, more difference is observed in the profiles of $\langle uv \rangle$ and $\langle w^2 \rangle$, so that it is difficult to specify a single location as a suitable candidate for the flow asymptotic state when the Reynolds stress convergence is used as the criterion. Notice that even though the flow area between $x/\delta_1 = 280$ and 320 is close to the domain exit in case IV, no effects due to the domain exit (indicated by the reduced growth rate of the integrated turbulence characteristics in the streamwise direction) are observed in the case IV results (Figs. 14(*b*) and supplemental Fig. S13 available in the Supplemental Materials).

Another criterion for the mixing layer self-similarity based on the total dissipation of the turbulent kinetic energy

$$\mathcal{E} = \int_{-L_y/2}^{L_y/2} \varepsilon \, dy = 2\nu \int_{-L_y/2}^{L_y/2} \left\langle \frac{\partial u_i}{\partial x_k} \frac{\partial u_j}{\partial x_k} \right\rangle dy \tag{8}$$

was proposed in Refs. [28] and [53]. This criterion requires $\mathcal{E}$ to be constant in the self-similar mixing layer. In the case IV simulation, $\mathcal{E}$ initially grows rapidly peaking at $x/\delta_1 \approx 180$ and then, reduces slowly toward the domain exit (Fig. 15(*a*)). That is, at $x/\delta_1 \approx 180$, three integral flow characteristics change their behavior: to the linear growth for the mixing layer thickness and K, and to monotonic decay (not to the constant value) for $\mathcal{E}$.

In Fig. 15(*b*), results for $\mathcal{E}$ from the case IV simulation are compared against data in spatially- and temporally developing turbulent mixing layers obtained in other DNS studies [22,28]. In the figure, the normalized $\mathcal{E}$ is plotted as a function of the Reynolds number based on the vorticity thickness, $\delta_\omega = \Delta U / (\partial \langle U \rangle / \partial y)_{\max}$. The total dissipation rate behaves similarly in the three simulations: reaching its maximum first and then, slowly converging toward values of $\mathcal{E} \sim 0.0045 - 0.005$. Close values of this parameter obtained in three DNS are remarkable given the simulations differences. However, the constant asymptotic value of $\mathcal{E}$ is not achieved in any of the three simulations, even though asymptotic turbulence statistics were reported in Refs. [22] and [28] as in this study.

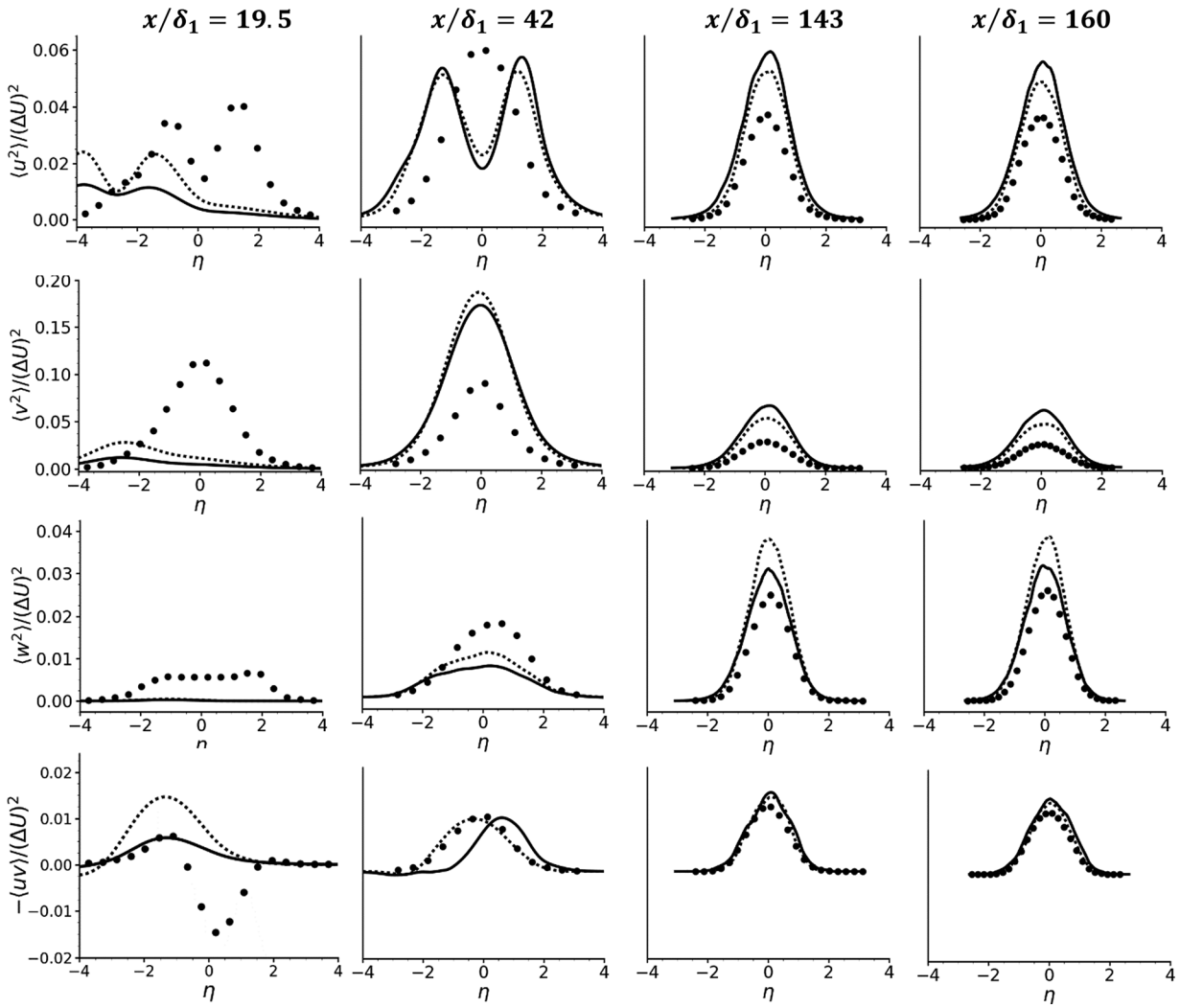

Fig. 11 Profiles of the Reynolds stresses at different locations in the streamwise direction for cases IV and V. Notations: — case IV, · · · · case V.

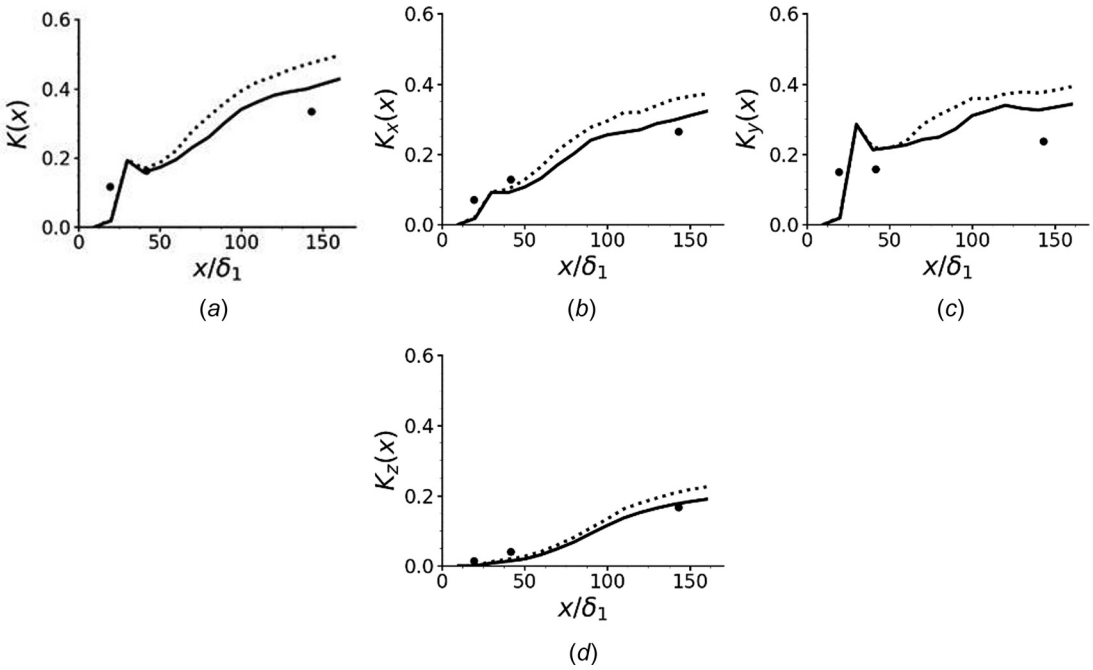

Fig. 12 Streamwise evolution of the flow characteristics integrated across the mixing layer in cases III and VI. Notations: — case III, · · · · case VI.

The results presented above show that the asymptotic state may not be reached simultaneously by all flow characteristics of interest, and when observed, it may be short-term lived. For these reasons, it is more accurate to refer to asymptotic states of families of flow characteristics rather than that of the flow. Of importance for this study focused on the computational domain dimensions is the observation that the analysis of asymptotic states of various flow parameters free from effects of the domain outlet boundary

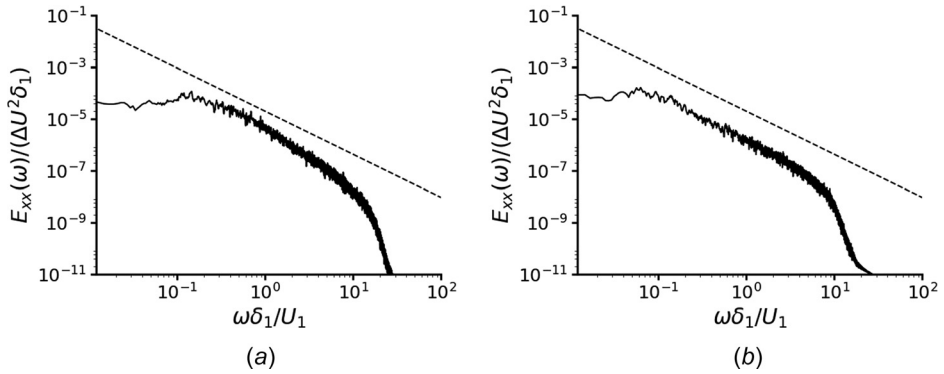

Fig. 13 One-dimensional energy spectrum at the flow centerline in case IV at (*a*) $x/\delta_1=150$, (*b*) $x/\delta_1=325$. The dashed line shows (–5/3)-slope.

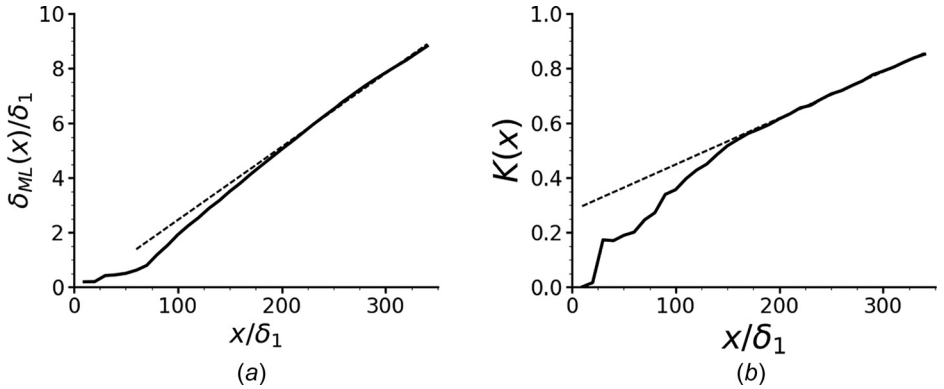

Fig. 14 Streamwise evolution of (*a*) mixing layer thickness and (*b*) integral turbulent kinetic energy in case IV. Dashed lines show a constant slope.

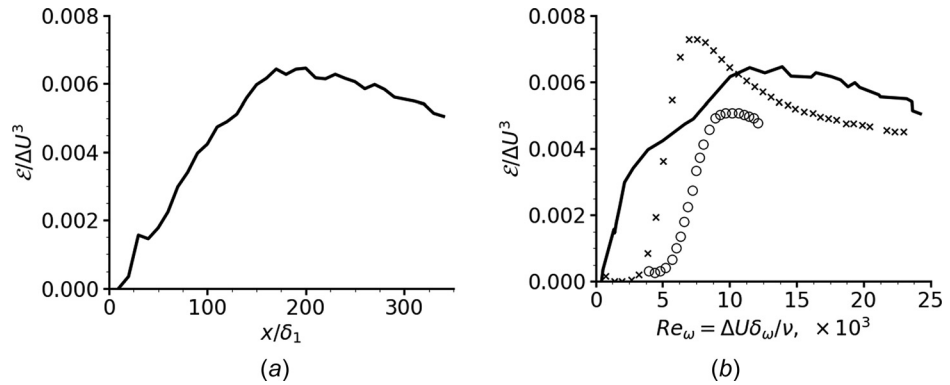

Fig. 15 Evolution of the turbulent kinetic energy dissipation rate integrated across the mixing layer (*a*) in the streamwise direction, (*b*) as a function of the local Reynolds number. Notations: — current DNS data, × - DNS data from Ref. [22], ○ – DNS data from Ref. [28].

conditions requires simulations to be conducted in a considerably long domain in the streamwise direction. In our study, the domain with $L_x/\delta_1 = 170$ is not sufficiently long for such a task, but the case IV domain with $L_x/\delta_1 = 350$ suits this purpose.

Conclusions

Prediction of the flow development using data from simulations ideally requires independence of the simulation results from numerical parameters. In this study, requirements for the computational domain dimensions in DNS of a planar spatially developing incompressible turbulent mixing layer were analyzed to achieve independency of the collected statistics from the domain dimensions. Previous studies, numerical and experimental, pointed toward the sensitivity of collected data to the domain dimensions, but solutions independent from the domain dimensions were not obtained and a systematic study of this issue is missing. This study contributes to that by varying the computational domain dimensions in all three directions and in larger ranges than in previous simulations Larger set of statistics is collected, with the data being statistically converged. The simulations were conducted for a spatially developing flow, which is of practical importance, but rarely previously attempted, and the problem statement is such that can be reproduced by others without introducing uncertainty associated with artificial turbulence.

In the simulations conducted for this study, the mixing layer developed between two coflowing laminar boundary layers formed on two sides of the sharp-ended splitter plate of a finite thickness. A total of six computational domains of similar geometry, but different dimensions in the three directions were used in the simulations, with the boundary layer characteristics at the trailing edge of the splitter plate closely matching those from experiments [11,37]. Two structured grids were generated. Both grids comply with the state-of-the-art requirements for a DNS grid, but one of the grids has finer resolution in the splitter plate wake area.

Multiple statistics were collected for the study at various locations inside the domain including the mean velocity component in the streamwise direction, scalar parameters integrated across the mixing layer, Reynolds stresses, and two-point correlations among others. These are parameters typically used to characterize the mixing layer development. The data analysis revealed different responses of different statistics to variations in the computational domain dimensions, with some of the statistics reaching independence from the domain dimensions and others not in the considered cases. A flow region also plays its role, with the same flow characteristics responding differently to variations in the domain dimensions depending on whether the data is sampled close to the splitter plate trailing edge, or where the mixing layer undergoes transition to turbulence, or where the mixing layer is fully turbulent (far from the splitter plate).

In particular, all considered statistics including the mean velocity profiles were found to be sensitive to variations of the domain dimension in the streamwise direction. However, the effects vary depending on the flow area. In the areas of the splitter plate wake and the flow transition to turbulence, all parameters are sensitive to this domain dimension. Increase of the domain size in the streamwise direction delays the flow mixing and transition to turbulence. When the mixing layer is fully turbulent, parameters associated with the spanwise direction and those characterizing the mixing layer growth are affected by the domain dimension in the streamwise direction. Other effects observed in the turbulent flow area in the shorter domain were found to be caused by the domain exit proximity. In the longer domain, the domain exit effects were not detected.

Scalar statistics and those associated with the streamwise direction were found to be less sensitive to the domain dimension in the transverse direction than the turbulent statistics associated with velocity fluctuations in the transverse and spanwise directions. The former group of statistics became independent of the domain dimension in the transverse direction in the midsized domain. The latter group of statistics showed some signs of variability even in the largest of considered domains in the transverse direction, equal to the experimental chamber dimension.

The flow area in the proximity of the splitter plate was also found sensitive to variations in the domain dimension in the spanwise direction. In the turbulent flow area, the Reynolds stress in the spanwise direction remains sensitive to the domain dimension in the spanwise direction toward the domain exit.

Overall, all three dimensions of the domain have strong effects on the flow development. The flow area in the wake of the splitter plate is the most sensitive to variations in all three domain dimensions. When the mixing layer becomes turbulent, one may expect statistics associated with velocity fluctuations in the spanwise direction to vary with the domain dimensions in the streamwise and spanwise directions. Large domains in the streamwise direction are beneficial for ensuring independence of the majority of flow characteristics of interest and for reducing effects of the domain exit.

Criteria to determine the domain dimensions in the spanwise and transverse directions that would guarantee independence of flow characteristics (Eqs. (5) and (6) in this paper) proposed previously in Refs. [21], [22], and [39], were tested in this study, but were found to be of limited use, that is, applicable to some statistics, but not to all. Based on the results of this study, it appears that no such criteria for the domain dimensions in the streamwise and spanwise directions may exist to guarantee independence of all flow parameters unless some limiters on the flow development are implemented in the flow geometry. In this regard, studies on the boundary condition effects will be the most beneficial as the next step.

In addition, the grid resolution was found to influence the streamwise evolution of the flow parameters. Effects of the grid stretching in the transverse direction require particular attention in this regard and have to be analyzed in depth in future studies.

The study also determined the computational domain dimensions suitable for studies of the turbulent mixing layer self-similarity. It was found that (i) different flow characteristics reach their asymptotic states at different locations within the flow, (ii) asymptotic states appear to be short-term lived for turbulence statistics, and (iii) a considerably long domain in the streamwise direction is required to observe such states.

Overall, the results of this study combined with our previous works [18,42] bring awareness to the sensitivity of DNS results to variations in the numerical procedure parameters. Achieving the grid resolution at the current state-of-the-art level and obtaining the statistically converged solution are necessary, but not sufficient steps to ensure the DNS solution uniqueness. This observation is likely to be valid for DNS of any flow, not only for the spatially developing mixing layer considered in the paper.

For practical purposes, an effort should be made to identify a set of statistics from DNS of a given flow that is less responsive to variations in the numerical procedure. Then, using the sensitivity analysis, the numerical procedure parameters should be determined that guarantee unchanged values of those statistics. Only after that, the values of these statistics can be used with confidence for prediction and validation of other computational approaches to study fluid flows.

Acknowledgment

Resources supporting this work were provided by the NASA High-End Computing (HEC) Program through the NASA Advanced Supercomputing (NAS) Division at Ames Research Center.

Data Availability Statement

The datasets generated and supporting the findings of this article are obtainable from the corresponding author upon reasonable request.

Nomenclature

E_{ij} = energy spectrum
h = thickness of the splitter plate at the trailing edge
k = turbulent kinetic energy, $0.5\sum_i \langle u_i^2 \rangle$
K = turbulent kinetic energy integrated across the mixing layer, $0.5(K_x + K_y + K_z)$
K_x, K_y, K_z = normal Reynolds stresses integrated across a mixing layer at a given streamwise location
L_x, L_y, L_z = computational domain dimension in the streamwise, transverse, and spanwise directions
L_x^{ML} = length of the mixing layer region in the computational domain
N = polynomial order of the Lagrange interpolants
N_s = number of snapshots
p = pressure
r_y, r_z = distances between two points in the transverse and spanwise directions
R_{ij} = two-point spatial correlations
Re_δ = Reynolds number with respect to the boundary layer thickness, $U_\infty \delta_{99}/\nu$
Re_θ = Reynolds number with respect to the boundary layer momentum thickness, $U_\infty \theta/\nu$
Re_ω = Reynolds number with respect to the mixing layer vorticity thickness, $\Delta U \delta_\omega/\nu$
$\mathbf{u}$ = instantaneous velocity vector
U, V, W = streamwise, transverse, and spanwise components of the instantaneous flow velocity
u_i = velocity fluctuations (u, v, w) in the streamwise, transverse, and spanwise directions
$\langle u_i u_j \rangle$ = Reynolds stresses
U_c = centerline velocity, $(U_1 + U_2)/2$
U_1, U_2 = free-stream velocity of high- and low-speed streams, respectively
U_∞ = free-stream velocity
x_i = streamwise (x), transverse (y), and spanwise (z) coordinates
y_0 = mixing layer centerline
δ_{ML} = mixing layer thickness
δx_i = average spacing between quadrature points within a grid element in a given direction
$\delta_\omega, \delta_{\omega,\max}$ = mixing layer vorticity thickness, $\Delta U/(\partial \langle U \rangle/\partial y)$ and its maximum value
δ_1 = boundary layer thickness at the splitter plate trailing edge on the high-velocity side in experiments [11]
δ_{99} = boundary layer thickness at the splitter plate trailing edge (any side)
Δt = time step
ΔU = velocity difference, $U_1 - U_2$
Δx_i = grid spacing in a given direction
ε = dissipation rate of the turbulent kinetic energy
η = normalized transverse coordinate, $(y - y_0)/\delta_{\mathrm{ML}}$
η_K, τ_K = Kolmogorov length and time scales
$\theta, \theta_{\max}$ = momentum thickness, $\left(1/\Delta U^2\right)\int_{-\infty}^{\infty}(U_1 - \langle U \rangle)(\langle U \rangle - U_2)\, dy$, and its maximum value
ν = kinematic viscosity
ρ = fluid density
τ_f = flow-through time, L_x^{ML}/U_c
ω = vorticity
∇ = gradient operator
$\langle \ldots \rangle$ = averaged value of a quantity

References

[1] Liepmann, H. W., and Laufer, J., 1947, "Investigations of Free Turbulent Mixing," NASA Technical Report No. 1257.
[2] Wygnanski, I., and Fiedler, H. E., 1970, "The Two-Dimensional Mixing Region," J. Fluid Mech., **41**(2), pp. 327–361.
[3] Brown, G. L., and Roshko, A., 1974, "On Density Effects and Large Structure in Turbulent Mixing Layers," J. Fluid Mech., **64**(4), pp. 775–816.
[4] Oster, D., Wygnanski, I., and Fiedler, H., 1977, "Some Preliminary Observations on the Effect of Initial Conditions on the Structure of the Two-Dimensional Turbulent Mixing Layer," Turbulence in Internal Flows: Turbomachinery and Other Engineering Applications; Proceedings of the SQUID Workshop, Warrenton, Va., June 14, 15, 1976. (A78-34826 14-34) Washington, DC, Hemisphere Publishing Corp., pp. 67–84.
[5] Weller, H. G., Tabor, G., Gosman, A. D., and Fureby, C., 1998, "Application of a Flame-Wrinkling LES Combustion Model to a Turbulent Mixing Layer," Proc. Int. Symp. Combust., **27**(1), pp. 899–907.
[6] Yoder, D. A., DeBonis, J. R., and Georgiadis, N. J., 2015, "Modeling of Turbulent Free Shear Flows," Comput. Fluids, **117**, pp. 212–232.
[7] Browand, F. K., and Latigo, B. O., 1979, "Growth of the Two-Dimensional Mixing Layer From a Turbulent and Nonturbulent Boundary Layer," Phys. Fluids, **22**(6), pp. 1011–1019.
[8] Ho, C. M., and Huerre, P., 1984, "Perturbed Free Shear Layers," Ann. Rev. Fluid Mech., **16**(1), pp. 365–422.
[9] Mehta, R., 1991, "Effect of Velocity Ratio on Plane Mixing Layer Development: Influence of the Splitter Plate Wake," Exp. Fluids, **10**(4), pp. 194–204.
[10] McMullan, W. A., Gao, S., and Coats, C. M., 2009, "The Effect of Inflow Conditions on the Transition to Turbulence in Large Eddy Simulations of Spatially Developing Mixing Layers," Intl. J. Heat Fluid Flow, **30**(6), pp. 1054–1066.
[11] Bell, J. H., and Mehta, R. D., 1990, "Development of a Two-Stream Mixing Layer From Tripped and Untripped Boundary Layers," AIAA J, **28**(12), pp. 2034–2042.
[12] Slessor, M. D., Bond, C. L., and Dimotakis, P. E., 1998, "Turbulent Shear-Layer Mixing at High Reynolds Numbers: Effects of Inflow Conditions," J. Fluid Mech., **376**, pp. 115–138.
[13] Vreman, B. E. R. T., Geurts, B., and Kuerten, H. A. N. S., 1997, "Large-Eddy Simulation of the Turbulent Mixing Layer," J. Fluid Mech., **339**, pp. 357–390.
[14] McMullan, W. A., and Garrett, S. J., 2016, "Initial Condition Effects on Large Scale Structure in Numerical Simulations of Plane Mixing Layers," Phys. Fluids, **28**(1), p. 015111.
[15] Sandham, N. D., and Sandberg, R. D., 2009, "Direct Numerical Simulation of the Early Development of a Turbulent Mixing Layer Downstream of a Splitter Plate," J. Turbul., **10**(1), pp. 1–17.
[16] Laizet, S., Lardeau, S., and Lamballais, E., 2010, "Direct Numerical Simulation of a Mixing Layer Downstream a Thick Splitter Plate," Phys. Fluids, **22**(1), p. 015104.
[17] Moin, P., and Mahesh, K., 1998, "Direct Numerical Simulation: A Tool in Turbulence Research," Ann. Rev. Fluid Mech., **30**(1), pp. 539–578.
[18] Colmenares, F. J. D., Poroseva, S. V., Peet, Y. T., and Murman, S. M., 2017, "DNS of a Spatially Developing Turbulent Mixing Layer From Co-Flowing Laminar Boundary Layers," AIAA Paper No. 2017-3641.

[19] Ko, J., Lucor, D., and Sagaut, P., 2008, "Sensitivity of Two-Dimensional Spatially Developing Mixing Layers With Respect to Uncertain Inflow Conditions," Phys. Fluids, **20**(7), p. 077102.
[20] Moser, R. D., and Rogers, M., 1993, "The Three-Dimensional Evolution of a Plane Mixing Layer: Pairing and Transition to Turbulence," J. Fluid Mech., **247**, pp. 275–320.
[21] Wang, Y., Tanahashi, M., and Miyauchi, T., 2007, "Coherent Fine Scale Eddies in Turbulence Transition of Spatially-Developing Mixing Layer," Int. J. Heat Fluid Flow, **28**(6), pp. 1280–1290.
[22] Attili, A., and Bisetti, F., 2012, "Statistics and Scaling of Turbulence in a Spatially Developing Mixing Layer at $Re_\lambda = 250$," Phys. Fluids, **24**(3), p. 035109.
[23] Comte, P., Lesieur, M., and Lamballais, E., 1992, "Large- and Small-Scale Stirring of Vorticity and a Passive Scalar in a 3-D Temporal Mixing Layer," Phys. Fluids A, **4**(12), pp. 2761–2778.
[24] Tanahashi, M., Iwase, S., and Miyauchi, T., 2001, "Appearance and Alignment With Strain Rate of Coherent Fine Scale Eddies in Turbulent Mixing Layer," J. Turbul., **2**, p. N6.
[25] Takamure, K., Ito, Y., Sakai, Y., Iwano, K., and Hayase, T., 2018, "Momentum Transport Process in the Quasi Self-Similar Region of Free Shear Mixing Layer," Phys. Fluids, **30**(1), p. 015109.
[26] Itoh, T., Naka, Y., Minamoto, Y., Shimura, M., and Tanahashi, M., 2018, "Large-Scale Clustering of Coherent Fine-Scale Eddies in a Turbulent Mixing Layer," Int. J. Heat Fluid Flow, **72**, pp. 100–108.
[27] Rogers, M. M., and Moser, R. D., 1992, "The Three-Dimensional Evolution of a Plane Mixing Layer: The Kelvin-Helmholtz Rollup," J. Fluid Mech., **243**(-1), pp. 183–226.
[28] Rogers, M. M., and Moser, R. D., 1994, "Direct Simulation of a Self-Similar Turbulent Mixing Layer," Phys. Fluids, **6**(2), pp. 903–923.
[29] Attili, A., and Bisetti, F., 2013, "Fluctuations of a Passive Scalar in a Turbulent Mixing Layer," Phys. Rev. E, **88**, p. 033013.
[30] Attili, A., Cristancho, J. C., and Bisetti, F., 2014, "Statistics of the Turbulent/Non-Turbulent Interface in a Spatially Developing Mixing Layer," J. Turbul., **15**(9), pp. 555–568.
[31] Laizet, S., and Lamballais, E., 2006, "Direct Numerical Simulation of a Spatially Evolving Flow From an Asymmetric Wake to a Mixing Layer," *Direct and Large-Eddy Simulation VI*, E. Lamballais, R. Friedrich, B. J. Geurts, O. Métais, eds., Springer, Dordrecht, The Netherlands, pp. 446–474.
[32] Fathali, M., Meyers, J., Rubio, G., Smirnov, S., and Baelmans, M., 2008, "Sensitivity Analysis of Initial Condition Parameters on the Transitional Temporal Turbulent Mixing Layer," J. Turbul., **9**, p. N12.
[33] Townsend, A., 1976, *The Structure of Turbulent Shear Flow. Cambridge Monographs on Mechanics*, Cambridge University Press, New York.
[34] Dimotakis, P. E., 1991, "Turbulent Free Shear Layer Mixing and Combustion," *High-Speed-Flight Propulsion Systems*, *in Progress in Astronautics and Aeronautics*, S. N. B. Murthy and E. T. Curran, eds., Vol. 137, American Institute of Aeronautics Astronautics, Washington, DC, pp. 265–340.
[35] Narayanan, S., and Hussain, F., 1996, "Measurements of Spatiotemporal Dynamics in a Forced Plane Mixing Layer," J. Fluid Mech., **320**(-1), pp. 71–115.
[36] Dimotakis, P. E., and Brown, G. L., 1976, "The Mixing Layer at High Reynolds Number: Large-Structure Dynamics and Entrainment," J. Fluid Mech., **78**(3), pp. 535–560.
[37] Bell, J. H., and Mehta, R. D., 1989, "Design and Calibration of the Mixing Layer and Wind Tunnel," Department of Aeronautics and Astronautics, Stanford University, Stanford, CA, Standard No. JIAA No. TR-89.
[38] Dziomba, B., and Fiedler, H. E., 1985, "Effect of Initial Conditions on Two-Dimensional Free Shear Layers," J. Fluid Mech., **152**, pp. 419–442.
[39] McMullan, W. A., 2015, "Spanwise Domain Effects on the Evolution of the Plane Turbulent Mixing Layer," Int. J. Comp. Fluid Dyn., **29**(6–8), pp. 333–345.
[40] Biancofiore, L., 2014, "Crossover Between Two- and Three-Dimensional Turbulence in Spatial Mixing Layers," J. Fluid Mech., **745**, pp. 164–179.
[41] Balaras, E., Piomelli, U., and Wallace, J. M., 2001, "Self-Similar States in Turbulent Mixing Layers," J. Fluid Mech., **446**, pp. 1–24.
[42] Colmenares, F. J. D., Poroseva, S. V., Peet, Y. T., and Murman, S. M., 2018, "Analysis of Uncertainty Sources in DNS of a Turbulent Mixing Layer Using Nek5000," AIAA Paper No. 2018-3226.
[43] Patera, A. T., 1984, "A Spectral Element Method for Fluid Dynamics: Laminar Flow in a Channel Expansion," J. Comp. Phys., **54**(3), pp. 468–488.
[44] Fischer, P., Kruse, J., Mullen, J., Tufo, H., Lottes, J., and Kerkemeier, S., 2008, "NEK5000: Open Source Spectral Element CFD Solver," Argonne National Laboratory, Lemont, IL, accessed on June 28, 2023, https://nek5000.mcs.anl.gov
[45] Ohlsson, J., Schlatter, P., Fischer, P. F., and Henningson, D. S., 2010, "Direct Numerical Simulation of Separated Flow in a Three-Dimensional Diffuser," J. Fluid Mech., **650**, pp. 307–318.
[46] Vinuesa, R., Hosseini, S. M., Hanifi, A., Henningson, D. S., and Schlatter, P., 2015, "Direct Numerical Simulation of the Flow Around a Wing Section Using High-Order Parallel Spectral Methods," Proceedings of the Ninth International Symposium on Turbulence and Shear Flow Phenomena, Melbourne, Australia, June 30–July 3, Paper No. 2B-3.
[47] Schlatter, P., and Örlü, R., 2012, "Turbulent Boundary Layers at Moderate Reynolds Numbers: Inflow Length and Tripping Effects," J. Fluid Mech., **710**, pp. 5–34.
[48] Sillero, J. A., Jiménez, J., and Moser, R. D., 2013, "One-Point Statistics for Turbulent Wall-Bounded Flows at Reynolds Numbers Up to $\delta+ \approx 2000$," Phys. Fluids, **25**(10), p. 105102.
[49] Pope, S. B., 2000, *Turbulent Flows*, Cambridge University Press, Cambridge.
[50] Delville, J., Ukeiley, L., Cordier, L., Bonnet, J. P., and Glauser, M., 1999, "Examination of Large-Scale Structures in a Turbulent Plane Mixing Layer: Part 1—Proper Orthogonal Decomposition," J. Fluid Mech., **391**, pp. 91–122.
[51] Mansour, N. N., Ferziger, J. H., and Reynolds, W. C., 1978, "Large-Eddy Simulation of a Turbulent Mixing Layer," Thermosciences Division, Department of Mechanical Engineering, Stanford University, Stanford, CA, Report No. TF-11.
[52] Bell, J., and Mehta, R., 1989, "Three-Dimensional Structure of a Plane Mixing Layer," AIAA Paper No. 89–0124.
[53] Clark, T. T., and Zhou, Y., 2003, "Self-Similarity of Two Flows Induced by Instabilities," Phys. Rev. E, **68**(6), p. 066305.